The instability of a South Polar Cap on Mars composed of carbon dioxide

Article · February 2014

DOI: 10.2172/8347

4 authors, including:

John Frederick Nye
University of Bristol
202 PUBLICATIONS **9,837** CITATIONS

SEE PROFILE

Icarus **144**, 449–455 (2000)
doi:10.1006/icar.1999.6306, available online at http://www.idealibrary.com on IDEAL®

The Instability of a South Polar Cap on Mars Composed of Carbon Dioxide

J. F. Nye

H. H. Wills Physics Laboratory, University of Bristol, Tyndall Avenue, Bristol BS8 1TL, England

W. B. Durham

Lawrence Livermore National Laboratory, University of California, P.O. Box 808, Livermore, California 94550
E-mail: durham1@llnl.gov

P. M. Schenk

Lunar and Planetary Institute, 3600 Bay Area Boulevard, Houston, Texas 77058

and

J. M. Moore

NASA Ames Research Center, Moffett Field, California 94035

Received February 1, 1999; revised July 23, 1999

If the martian south polar cap were composed of solid carbon dioxide, would it be sufficiently stable against collapse under its own weight? This question is examined in the light of new experiments on the creep of solid carbon dioxide and new high-resolution topographic mapping of the south polar cap. The conclusion from a simple model is that, with the strongest of three flow laws compatible with the measurements, CO_2 is strong enough to support a cap of this material with thickness about 1800 m for 10^7 years or more, which is the age suggested by the cratering record. However, none of the three possible flow laws will allow a 3000-m cap, the thickness suggested by stereogrammetry, to survive for 10^7 years, indicating that the south polar ice cap is probably not composed of pure CO_2 ice.

Key Words: **Mars; Mars, surface; ices; geophysics.**

1. THE PROBLEM

Spacecraft data indicate that the surface layers of the residual south polar ice deposit of Mars (Fig. 1a) probably consist of CO_2 ice (Paige *et al*. 1990) and are an important reservoir or sink for atmospheric CO_2 (or H_2O) over time. The extent to which the entire thickness of the south polar cap (and the surrounding layered deposits) could be composed of CO_2 ice is unknown. The hypothesis that the cap is made of solid carbon dioxide would have to be rejected if this material were so weak that a cap of the required thickness would quickly collapse under its own weight. Three factors stimulated a new look at this problem: the launch of the Mars Polar Lander in January 1999 to search for water and carbon dioxide ice near the south pole, new creep experiments on solid carbon dioxide (Durham *et al*. 1999), and new high-resolution stereo topography of the south pole (Schenk and Moore 2000).

A simple model is examined here to estimate the order of magnitude of the collapse time of a putative carbon dioxide polar cap on Mars. The problem is different from the classical glaciological one that assumes a steady state, because it is thought that there has been no significant accumulation or ablation in the past 10^7 years.

2. SHAPE, AGE, AND COMPOSITION OF THE SOUTH POLAR CAP

High-resolution Viking stereophotogrammetry measurements (Schenk and Moore 2000) show the south polar cap to be a distinct, approximately circular symmetric hump (Fig. 1b) 3000 ± 200 m high, with a radius of 225 ± 25 km. Crater densities suggest that the surface of the layered deposits, of which the polar cap is just a part, are at least 10^8 years old (Plaut *et al*. 1988). Although no counts were performed on the polar cap itself, it is also very sparsely cratered and is inferred to be 10^6 to 10^8 years old.

Recent topographic measurements from the Mars Orbiter Laser Altimeter (MOLA) (Smith *et al*. 1999) confirm the overall stereo-derived measurements of the shape and dimensions of the south polar dome (Schenk and Moore 2000). The MOLA topography also suggests but does not demonstrate that the basal

0019-1035/00 $35.00

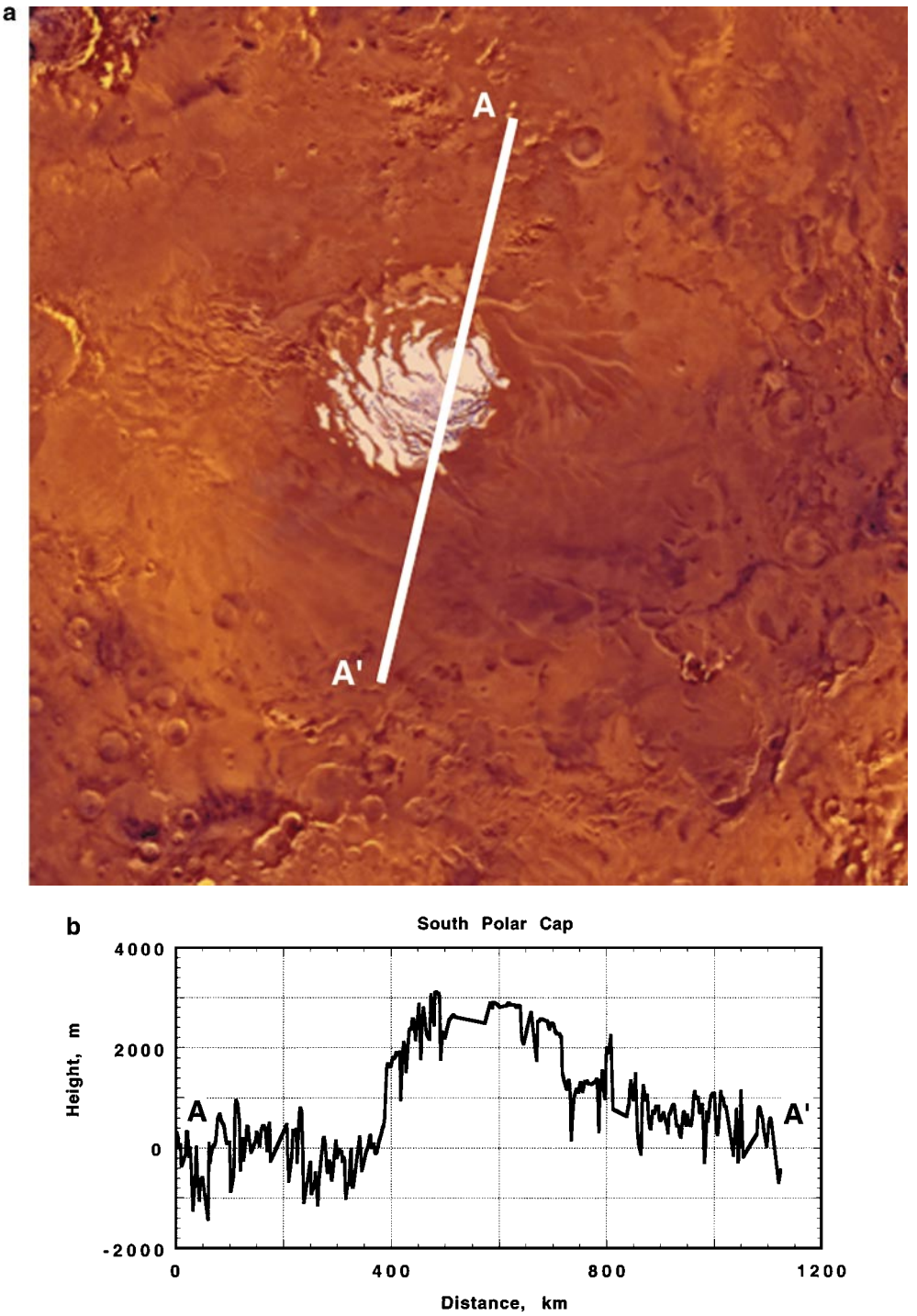

FIG. 1. (a) Color image mosaic of the south polar region of Mars, showing location of profile in (b) (line A–A′). Bright areas are covered by residual frost and ice deposits. South polar cap actually extends roughly 100 km beyond the edge of these deposits. The scene is centered on the south pole and is 2000 km across. (b) Topographic cross section across the south polar cap of Mars (from Schenk and Moore 1999). Profile begins in smooth deposits. The edge of the polar cap begins at ∼375 km distance and extends to ∼825 km. The right end of the profile is in layered deposits, which are elevated 1 to 2 km above the surrounding plains.

topography of the polar deposit may be deflected downward. The amount of flexure cannot be measured at present but could be as much as 2500 m or it could be negligible (Smith *et al*. 1999). A more detailed analysis of the role of basal topography in ice cap flow is beyond the scope of this work. For present purposes we shall assume a flat base for the cap. The consequences of a depressed basal topography are discussed at the end of this paper.

Although deep troughs and terraces cut into the surfaces of both domes and there is evidence that both deposits were once significantly larger in the distant past, the topographic profiles of the north and south polar ice caps have similar domed shapes (Zuber *et al*. 1998, Schenk and Moore 2000). The surface of the southern cap is scarred by a number of widely spaced concentric scarps, forming a series of descending terraces. These features suggest that the cap is currently undergoing erosion. The degree to which this shape is controlled by erosion is difficult to determine but the overall shape is suggestive of an equilibrium topographic profile of a mass deforming under its own weight. Future analyses may place improved constraints on the history of the south polar deposits. We assume that ablation and erosion has been volumetrically minor in the south polar deposit over the past 10^7 years.

The topographic center of the cap lies on the rim of an 800-km-wide impact basin (Schenk and Moore 2000), but this rim is narrow relative to the fairly flat top part of the dome. The broad symmetry and domed profile of the polar cap suggest that the upper surface does not significantly reflect this buried feature. Other than this rim, the terrains immediately surrounding the edge of the polar cap are relatively flat, suggesting that the local topography does not significantly affect flow within the ice cap itself.

3. THE FLOW LAW

Clark and Mullin (1976) looked at the question of a carbon dioxide polar cap on Mars but were hampered by a lack of reliable topographic data, which prevented them from knowing the true lateral and vertical extent of the south polar cap. They derived a flow law for CO_2 based on uniaxial compression experiments. They ran their tests without the benefit of confining pressure, so they were unable to guarantee suppression of processes involving change of volume, like fracturing and microfracturing. Therefore, their strength measurements must be considered lower bounds, leaving open the possibility that the strength under confining pressure is considerably greater.

New experiments by Durham *et al*. (1999) use similar uniaxial compression but in the presence of elevated confining pressure. They measure the differential stress σ required to maintain a constant displacement rate. The strain rate $\dot{\varepsilon}_1$ is assumed to be given by

$$\dot{\varepsilon}_1 = A_D \exp(-Q/R_G T)\sigma^n,$$

TABLE I
Computed Values for Different Flow Laws

	CO_2 ice (a)	CO_2 ice (b)	CO_2 ice (c)	H_2O ice (d)
A_D, $s^{-1}(MPa)^{-n}$	9.55×10^{-3}	4.37×10^{3}	1.202×10^{11}	9.00×10^{4}
n	2	4.5	7	3
Q, J/mol	15,000	31,000	59,000	60,000
C, yr^{-1} m^{-n}	5.85×10^{-4}	3.79×10^{-8}	5.72×10^{-14}	7.94×10^{-13}
$\tau(r = 0.5\ R_0)$, MPa	0.111	0.126	0.129	0.071

where R_G is the gas constant, and most of the results fit this equation with the values of the material constants, A_D, n, and Q, shown in column (b) of Table I. However, as the authors discuss in their paper, there is considerable uncertainty in the value of n. Repeated anomalies in the experimental data indicate that n may be 7 or higher, while theoretical arguments, as well as experience with other crystalline materials in the geologic setting suggest that n could be much lower than 4.5 at the low stresses *in situ*. Deformation mechanisms such as grain boundary sliding (e.g., Goldsby and Kohlstedt 1997) are favored at low stresses and can have n values of 2 or less. To allow for all reasonable possibilities the alternative laws shown as (a) and (c) are also considered. Although the three laws look very different, because the values of A_D differ extremely, in fact they all agree at the lowest stresses used in the experiments; thus, the value of n decides the extrapolation from laboratory strain rates to the much slower ones in a martian cap. The experiments confirm that solid CO_2 is weaker than water ice by a factor of well over 10 and show that the measurements by Clark and Mullin (1976) underestimated the strength of CO_2 by a factor of only about 2.

The flow law thus measured by Durham *et al*. (1999) relates uniaxial compression rate $\dot{\varepsilon}_1$ to uniaxial compressive stress σ, while for the cap model it is necessary to relate the rate of simple shear $\dot{\gamma}$ to the shear stress τ_0. We write for the two kinds of flow law at a given temperature,

$$\dot{\varepsilon}_1 = B\sigma^n \qquad \text{and} \qquad \dot{\gamma} = D\tau_0^n,$$

so that

$$B = A_D \exp(-Q/R_G T). \tag{1}$$

The transformation between them is made via the generalized flow law (Nye 1953, Paterson 1994) $\dot{\varepsilon} = A\tau^n$, where $\dot{\varepsilon}$ is the effective strain rate and τ is the effective shear stress, which is valid for all states of stress and strain rate. Here τ is constructed from the stress tensor σ_{ij} by defining the stress deviator $\sigma'_{ij} = \sigma_{ij} - \frac{1}{3}\sigma_{kk}$ and writing $2\tau^2 = \sigma'_{ij}\sigma'_{ij}$ (τ positive). In a similar way $\dot{\varepsilon}$ is constructed from the strain rate tensor $\dot{\varepsilon}_{ij}$ by writing $2\dot{\varepsilon}^2 = \dot{\varepsilon}_{ij}\dot{\varepsilon}_{ij}$ ($\dot{\varepsilon}$ positive). It then follows that

$$D = 3^{\frac{1}{2}(n+1)} B. \tag{2}$$

4. THE ICE CAP MODEL

Because we are concerned only with an order of magnitude for the decay time we shall ignore the curvature of the planet's surface and assume a circular cap resting on a plane horizontal base (Fig. 2). With a mean annual surface temperature of 155 K and estimates for heat flow based on a terrestrial model, the temperature gradient may be high enough to cause basal melting (at 217 K) of a CO_2 cap (Ross and Kargel 1998). Nevertheless, so as not to overestimate the rate of thinning, we shall assume a uniform temperature of 180 K and that the base is below the melting point; the latter means that there is no sliding on the base (Paterson 1994). It is assumed, therefore, that the deformation is predominantly by horizontal shearing within the ice.

At radius r and time t the thickness is $h(r, t)$. The thickness at the center $h(0, t)$ is denoted by $h_0(t)$ and the radius of the base is $r_0(t)$. The required solution of the flow equations, a similarity solution, was introduced into glaciology by Halfar (1981) for two-dimensional flow and (Halfar 1983) for radial flow, as here. Hindmarsh (1990) has discussed Halfar's two-dimensional solution. Here we first deduce Halfar's radial flow solution from a similarity hypothesis and then apply the result to the martian situation.

Defining a scaled radial coordinate $\rho = r/r_0(t)$ and a scaled thickness,

$$\eta = \frac{h(r,t)}{h_0(t)} = \frac{h(r_0\rho, t)}{h_0(t)} = \eta(\rho, t),$$

we look for a solution of the flow equations in which $\eta = \eta(\rho)$, independent of t; that is, the scaled shape always remains the same.

Let $q(r, t)$ be the radial flux (volume per unit time crossing an area of height h and unit circumferential length). Then conservation of volume requires that

$$\left(\frac{\partial(qr)}{\partial r}\right)_t + r\left(\frac{\partial h}{\partial t}\right)_r = 0, \tag{3}$$

the second term of which is

$$r\left(\frac{\partial h}{\partial t}\right)_r = r_0\rho\left(\frac{\partial(h_0\eta)}{\partial t}\right)_r = r_0\rho\left(\dot{h_0}\eta + h_0\frac{\mathrm{d}\eta}{\mathrm{d}\rho}\left(\frac{\partial\rho}{\partial t}\right)_r\right). \tag{4}$$

Because the overall volume is fixed and the scaled shape is fixed,

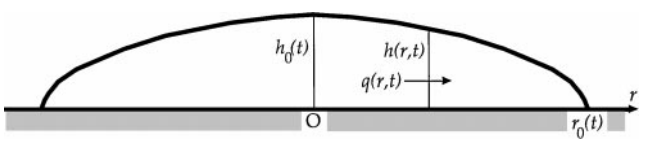

FIG. 2. The simplified model.

$\mathrm{d}/\mathrm{d}t(h_0 r_0^2) = 0$, and hence $\dot{r}_0 = -(r_0/2h_0)\dot{h_0}$. Since $\rho = r/r_0$,

$$\left(\frac{\partial\rho}{\partial t}\right)_r = -\frac{r}{r_0^2}\dot{r}_0 = \frac{\rho}{2h_0}\dot{h_0}.$$

Thus, from (4),

$$r\left(\frac{\partial h}{\partial t}\right)_r = r_0\rho\dot{h_0}\left(\eta + \frac{1}{2}\rho\frac{\mathrm{d}\eta}{\mathrm{d}\rho}\right) = \frac{1}{2}r_0\dot{h_0}\frac{\mathrm{d}}{\mathrm{d}\rho}(\rho^2\eta), \tag{5}$$

and Eq. (3) becomes, in terms of ρ,

$$\left(\frac{\partial(q\rho)}{\partial\rho}\right)_t + \frac{1}{2}r_0\dot{h_0}\frac{\mathrm{d}}{\mathrm{d}\rho}(\rho^2\eta) = 0. \tag{6}$$

The crucial step is in (5), where $(\partial/\partial t)_r$ is converted to $\mathrm{d}/\mathrm{d}\rho$. Equation (6) may now be integrated with respect to ρ at constant t; thus

$$q\rho + \frac{1}{2}r_0\dot{h_0}\cdot\rho^2\eta = \text{constant}.$$

Dividing by ρ and demanding that $q = 0$ at $\rho = 0$ sets the constant to zero.

We now use the flow relation (shallow ice approximation) (Nye 1952),

$$q = Ch^{n+2}(-\partial h/\partial r)_t^n = C\frac{h_0^{2n+2}}{r_0^n}\cdot\eta^{n+2}(-\mathrm{d}\eta/\mathrm{d}\rho)^n, \tag{7}$$

where

$$C = D(\rho' g)^n/(n+2). \tag{8}$$

ρ' is the density, and the full stop in (7) separates the time-dependent part from the ρ-dependent part. At the extreme edge the slope becomes infinite and the assumed relation (7) must break down; it should be replaced by different physics, but because the region affected is very narrow we shall ignore this defect. A similar problem arises in all models of this kind. The equation to be integrated is therefore

$$C\frac{h_0^{2n+2}}{r_0^n}\cdot\eta^{n+2}(-\mathrm{d}\eta/\mathrm{d}\rho)^n + \frac{1}{2}r_0\dot{h_0}\cdot\rho\eta = 0. \tag{9}$$

The variables may now be separated to give

$$2C\eta^{n+1}(-\mathrm{d}\eta/\mathrm{d}\rho)^n = K\rho \tag{10}$$

and

$$\dot{h_0} = -K\left(h_0^{2n+2}/r_0^{n+1}\right), \tag{11}$$

where K is a constant.

The profile follows from integrating (10). First, require that $\eta = 0$ at $\rho = 1$,

$$-\int_1^0 \eta^{1+1/n} d\eta = \left(\frac{K}{C}\right)^{1/n} \int_0^1 \rho^{1/n} d\rho,$$

from which

$$K = 2C\left(\frac{n+1}{2n+1}\right)^n. \tag{12}$$

Then the scaled profile is

$$\rho^{1+1/n} + \eta^{2+1/n} = 1, \tag{13}$$

as found by Halfar (1983). It is worth noting that, if the base were assumed to be not horizontal but depressed by a constant fraction f of the overlying height, the only difference is that h, h_0, and η refer to the thickness rather than the elevation and C is replaced by $C(1-f)^n$ throughout. In particular, the relation between ρ and η in (13) is not changed.

Integration of (11) gives the time dependence. It is convenient to think of $t = 0$ as the present, when the central height is H_0 and the radius of the cap is R_0 say. Then $h_0 r_0^2 = \text{constant} = H_0 R_0^2$, and (11) becomes

$$\dot{h_0} = -K\left(H_0 R_0^2\right)^{-(n+1)/2} h_0^{(5/2)(n+1)}.$$

This integrates to give the decay of the central height as

$$h_0(t) = H_0\left(1 + \frac{t}{t_0}\right)^{-2/(5n+3)}, \tag{14}$$

with, using (12),

$$t_0 = \frac{1}{C(5n+3)} \cdot \left(\frac{2n+1}{n+1}\right)^n \cdot \frac{R_0^{n+1}}{H_0^{2n+1}}. \tag{15}$$

$t = -t_0$ is the time at which the central height is asymptotically infinite (Fig. 3). Since $H_0 R_0^2$ is constant the corresponding equation for the expansion of the outer rim is

$$r_0(t) = R_0\left(1 + \frac{t}{t_0}\right)^{1/(5n+3)}, \tag{16}$$

and the aspect ratio diminishes according to

$$\frac{h_0(t)}{r_0(t)} = \frac{H_0}{R_0}\left(1 + \frac{t}{t_0}\right)^{-3/(5n+3)}. \tag{17}$$

In Eq. (15) C, R_0, and H_0 are observed quantities, and so t_0 can be calculated. In this model the profile of the cap decays steadily from an initial δ-function at $t = -t_0$, but always retaining the same scaled shape. Of course, the real history of the martian southern polar cap was not this, but the justification for using such a simple model is that, as Halfar (1983) has shown, the scaled profile is stable against all perturbations that preserve the total volume. Thus, whatever the actual genesis, the surface may be expected to have settled down quite quickly (in a time much less than t_0) to the steady profile calculated (much as molasses falling off a spoon onto a plate quickly forms a dome shape). We can say that, if the actual cap is more than 10^7 years old, it means that $t_0 > 10^7$ years.

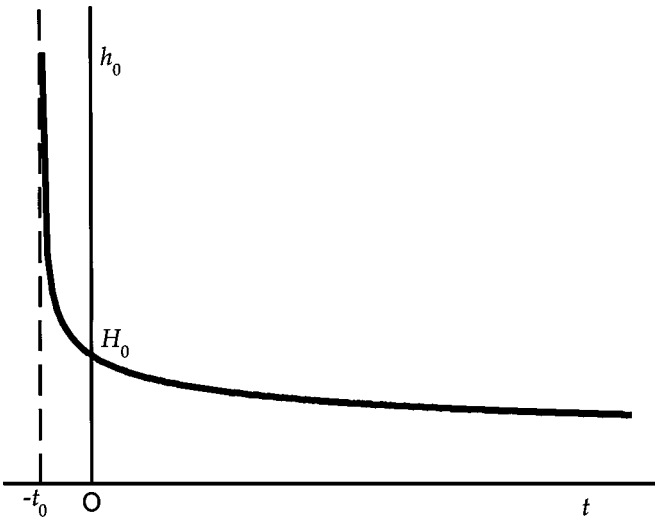

FIG. 3. Time dependence of the central height h_0.

5. NUMERICAL VALUES USED

The values used were $R_0 = 200$ km, $H_0 = 3000$ m, $\rho' = 1560\,\text{kg m}^{-3}$, $g = 3.72\,\text{m s}^{-2}$, $T = 180$ K. The first three columns of Table I show the constants for the three flow laws (a), (b), and (c) for solid CO_2. For comparison, column (d) of the table shows the corresponding constants for H_2O ice at the same temperature. The flow law used for H_2O ice is that recommended by Paterson (1994) (see below for alternatives). The fourth line of the table gives the values of C obtained by using Eqs. (1), (2), and (8).

6. PROFILE AND DISCUSSION

Figure 4 shows the scaled profiles computed from Eq. (13) for the four flow laws. The scaled profiles depend only on n and not on C. They are all quite similar and may be compared with the parabolic profile $\eta = (1-\rho)^{\frac{1}{2}}$ corresponding to the assumption of perfect plasticity (Orowan 1949, Nye 1951). The approach to the limit $n \to \infty$ is clearly seen. The curves with finite n all have zero slope at the summit, in contrast with the parabola which does not. The parabola is then necessarily below the other curves. The present basal shear stress $\tau = \rho' g h(-\partial h/\partial r)$ is much the same for all the CO_2 flow laws, but it is smaller for water ice because of its lower density. The values of τ at $r = 0.5R_0$ are shown in the last line of the table.

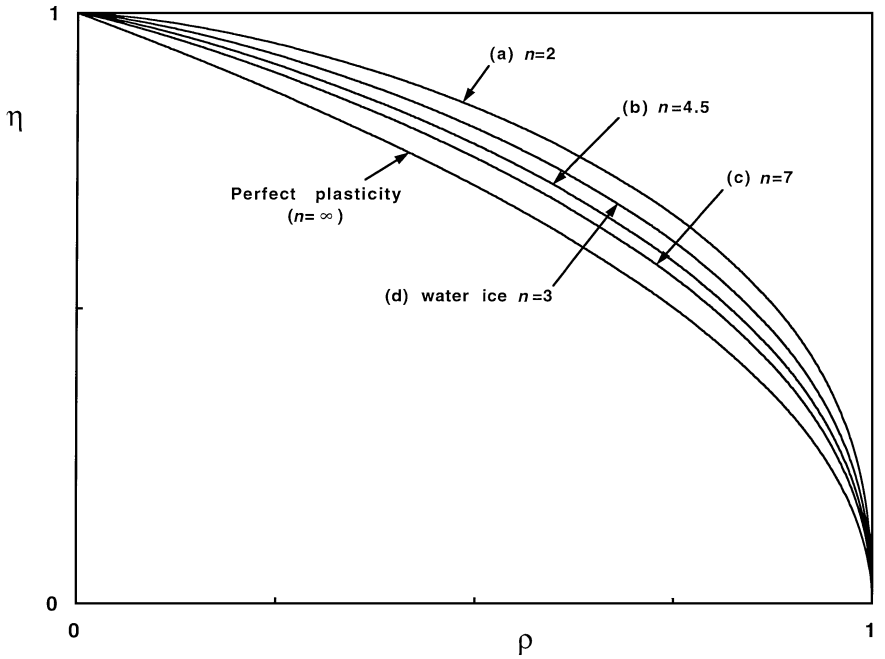

FIG. 4. Scaled profiles. The flow laws are as in Table I, with an additional parabolic curve for perfect plasticity.

Figure 5 plots t_0 against H_0 from (15) for these three different assumptions about the flow law for CO_2 and for water ice. The broken line drawn at $t_0 = 10^7$ years, the inferred minimum age, shows that even with the strongest of the three flow laws for CO_2 (law (c)) the height would be merely 1840 m after this length of time; alternatively, the broken line drawn at $H_0 = 3000$ m, the thickness suggested by stereogrammetry, shows that a cap of this height could have an age of 6700 years at most.

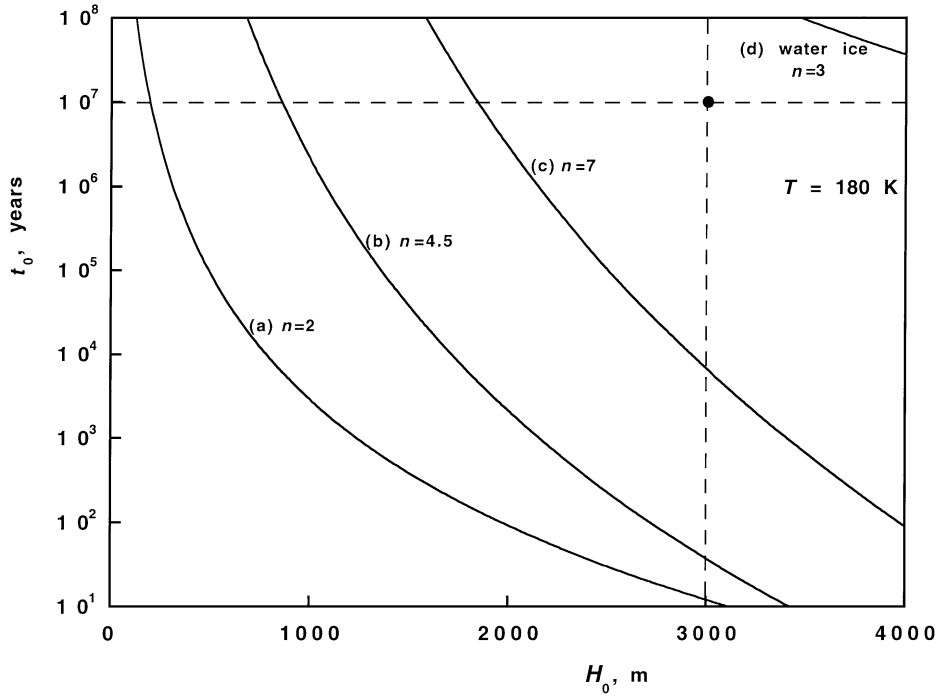

FIG. 5. The age t_0 versus the central height H_0 at the present time $t = 0$. (a), (b), and (c) refer to the three flow laws for solid CO_2, and for water ice (d), given in Table I. The observed height and the assumed age are indicated ($R_0 = 200$ km).

On the other hand, Fig. 5 also shows that H_2O ice is quite strong enough to support a 3000-m ice cap. H_2O ice at the same uniform temperature of 180 K could support a height of 4800 m after 10^7 years. A similar conclusion follows for other ice flow laws. The flow law recommended by Durham *et al.* (1997) ($A_D = 1.26 \times 10^5$, $n = 4$, $Q = 61{,}000$, with units as in Table I) gives an even stronger ice cap, which could support a height of 5600 m after 10^7 years. If grain boundary sliding operates in ice under martian conditions, the ice cap becomes weaker and falls to $H_0 = 3730$ m after 10^7 years, based on the water ice flow law of Goldsby and Kohlstedt (1997) with grain size 1 mm ($A_D = 61.8$, $n = 1.8$, $Q = 49{,}000$, with units as in Table I). Thus the water-ice hypothesis is favored.

The model assumes a flat base. Figure 1b shows no evidence of any buried mountains, but positive elevation of the underlying terrain would mean that the surface of the cap is actually higher than is calculated here. The buried rim of Prometheus basin is only 10–20 km wide (Schenk and Moore 2000) and is not significant enough to affect our conclusions. Correspondingly, depression of the lower surface, as allowed in the recent MOLA observations (Smith *et al*. 1999), would lead to a lower elevation of the top surface. Viewed alternatively, holding the elevation of the modeled cap at the observed value of 3000 m, positive elevation of the underlying surface would mean a thinner ice layer is present and would therefore work against the conclusions presented here. Isostatic depression of the underlying surface, would indicate a thicker ice layer, reinforcing our conclusions.

We should also note that the experimental results for the flow law are for pure CO_2. Impurities, different grain sizes, preferred orientations, and so on would certainly have some effect (as they do in water ice), but they are perhaps unlikely to change the order of magnitude of the values computed for solid CO_2.

We conclude that the south polar cap probably consists of water ice, with an unknown admixture of dust.

ACKNOWLEDGMENTS

P.S. and J.M. gratefully acknowledge the support of Carol Stoker (NASA Ames Research Center). W.B.D. gratefully acknowledges NASA support under Order W-19,075; his portion of the work was performed under the auspices of the U.S. Department of Energy by the Lawrence Livermore National Laboratory under Contract W-7405-ENG-48. J.F.N. thanks Dr. Richard Hindmarsh for helpful correspondence which revealed the relevance of Halfar's similarity solution to the martian situation.

REFERENCES

Clark, B., and R. Mullin 1976. Martian glaciation and the flow of solid CO_2. *Icarus* **27**, 215–228.

Durham, W. B., S. H. Kirby, and L. A. Stern 1997. Creep of water ices at planetary conditions: A compilation. *J. Geophys. Res.* **102**, 16293–16302.

Durham, W. B., S. H. Kirby, and L. A. Stern 1999. Steady-state flow of solid CO_2: Preliminary results. *Geophys. Res. Lett.* **26**, 3493–3496.

Goldsby, D. L., and D. L. Kohlstedt 1997. Grain boundary sliding in fine-grained ice I. *Scr. Mater.* **37**, 1399–1406.

Halfar, P. 1981. On the dynamics of the ice sheets. *J. Geophys. Res.* **86**, 11,065–11,072.

Halfar, P. 1983. On the dynamics of the ice sheets 2. *J. Geophys. Res.* **88**, 6043–6051.

Hindmarsh, R. C. A. 1990. Time-scales and degrees of freedom operating in the evolution of continental ice-sheets. *Trans. R. Soc. Edinburgh: Earth Sci.* **81**, 371–384.

Nye, J. F. 1951. The flow of glaciers and ice-sheets as a problem in plasticity. *Proc. R. Soc. London A* **207**, 554–572 .

Nye, J. F. 1952. The mechanics of glacier flow. *J. Glaciol.* **2**, 82–93.

Nye, J. F. 1953. The flow law of ice from measurements in glacier tunnels, laboratory experiments and the Jungfraufirn borehole experiment. *Proc. R. Soc. London A* **219**, 477–489.

Orowan, E. 1949. Discussion meeting. *J. Glaciol.* **1**, 231–236.

Paige, D. A., K. E. Herkenhoff, and B. C. Murray 1990. Mariner 9 observations of the south polar cap of Mars: Evidence for residual CO_2 frost. *J. Geophys. Res.* **95**, 1319–1326.

Paterson, W. S. B. 1994. *The Physics of Glaciers*, 3rd ed. Pergamon, Oxford.

Plaut, J., R. Kahn, E. Guinness, and R. Arvidson 1988. Accumulation of sedimentary debris in the south polar region of Mars and implications for climate history. *Icarus* **75**, 357–377.

Ross, R. G., and J. S. Kargel 1998. Thermal conductivity of Solar System ices, with special reference to martian polar caps. In *Solar System Ices* (B. Schmitt, C. de Bergh, and M. Festou, Eds.), pp. 33–62. Kluwer, Dordrecht.

Schenk, P. M., and J. M. Moore 2000. Stereo topography of the south polar region of Mars: Volatile inventory and Mars polar lander landing site. *J. Geophys. Res.*, in press.

Smith, D. E., and 18 colleagues 1999. The global topography of Mars and implications for surface evolution. *Science* **284**, 1495–1503.

Zuber, M. T., and 20 colleagues 1998. Observations of the north polar region of Mars from the Mars Orbiter Laser Altimeter. *Science* **282**, 2053–2060.